CARBON 50 (2012) 3859–3867

Available at www.sciencedirect.com

SciVerse ScienceDirect

journal homepage: www.elsevier.com/locate/carbon

In situ characterization of structural changes and the fraction of aligned carbon nanotube networks produced by stretching

Shu Li [a], *Jin Gyu Park* [a], *Zhiyong Liang* [a,*], *Theo Siegrist* [b], *Tao Liu* [a], *Mei Zhang* [a], *Qunfeng Cheng* [a], *Ben Wang* [a], *Chuck Zhang* [a]

[a] *High-Performance Materials Institute, Florida State University, 2005 Levy Ave, Tallahassee, FL 32310, USA*
[b] *Department of Chemical and Biomedical Engineering, Florida State University, 2525 Pottsdamer Street, Tallahassee, FL 32310-6046, USA*

ARTICLE INFO

Article history:
Received 20 February 2012
Accepted 8 April 2012
Available online 13 April 2012

ABSTRACT

The mechanism of carbon nanotube (CNT) alignment during stretching was examined by the *in situ* characterization of carbon nanotube networks (CNTNs) under tensile strains using X-ray and Raman scattering techniques. A method of quantifying the inhomogeneous alignment of macroscopic CNTNs is explored based on bulk property measurements of their electrical anisotropy and X-ray diffraction diagrams. The results show that the process of stretch-induced alignment of CNTNs included straightening the waviness of the long nanotube ropes, as well as the self-assembling and denser packing of the nanotubes. For samples at a strain of 40%, the fraction of aligned nanotubes was as high as 0.85. The aligned fraction of CNTs serves as an important parameter for the quality control of the alignment process and numerical simulations of structure–property relationships of CNTNs and their composites.

1. Introduction

Carbon nanotubes (CNTs) possess excellent electrical [1], thermal [2], and mechanical [3] properties; however, because of the inherent anisotropy of their cylindrical structures, the performance of macroscopic carbon nanotube networks (CNTNs) is usually suppressed by the misalignment of constituent nanotubes. Researchers have studied various techniques to manipulate the orientation of carbon nanotubes. de Heer et al. [4] aligned pure CNTs by drawing suspension through a micropore filter. Zhang and Iijima [5] used argon gas flow inside the laser ablation reactor to align the nanotubes. Smith et al., [6] Chen et al., [7] and Kamat et al. [8] applied strong magnetic fields, alternating currents (AC) and direct current (DC) electric fields, respectively, during the filtration/deposition of CNT suspension to achieve alignment. And Martin et al. [9] aligned CNTs dispersed in epoxy resin with both AC and DC electric fields. While these methods successfully aligned nanotubes without the aid of other additives, the sample sizes were very limited and scaling up is not easily achieved. Other methods of nanotube alignment included the addition and mixture of polymer materials. Haggenmueller et al. [10] aligned CNTs in poly(methyl methacrylate) (PMMA) through solvent casting and melt mixing. Other researchers have tried various mechanical stretching techniques to align CNTs with the assistance of binder materials, including polyhydroxyaminoether (PHAE) [11], polyurethane acrylate (PUA) [12], polypropylene (PP) [13], and polyvinyl alcohol (PVA) [14,15]. The weight percentages of polymers in these composites were up to 50%, which significantly limited the properties of the resultant materials. On the other hand, the direct alignment of neat CNTs was only achieved through spinning of continuous CNT fibers either from the CVD furnace [16] or vertical nanotube arrays grown on substrates [17–20]. Recently, our group [21] demonstrated the stretching of macroscopic neat CNTNs of millimeter-long nanotubes that are commercially available.

* *Corresponding author.*
E-mail address: liang@eng.fsu.edu (Z. Liang).
0008-6223/$ - see front matter
http://dx.doi.org/10.1016/j.carbon.2012.04.029

A 40% elongated post-stretch multi-walled carbon nanotube (MWCNT) sheet yielded more than a 200% improvement in tensile strength, 22-fold improvement in Young's modulus, and 40% increase in electrical conductivity along the stretch direction. The exceptional properties achieved from the stretched CNTNs prompts the need to better understand the mechanism of CNT alignment under stretching strain. The assessment of the aligned fraction is of significant importance for both quality control of CNTN alignment and structure–property relationship studies of the aligned networks. The most frequently used technique of characterizing the alignment of fibers/fibrils using X-ray scattering was explored by Hermans [22,23] in 1946. Developed to derive the orientation of cellulose fibers, the degree of alignment as determined by the Hermans orientation function has been applied to the characterization of the alignment of micrometer long carbon nanotubes [24] and their polymer composites [13]. Recognizing that the X-ray study alone would overestimate the unaligned fraction of CNTs, Fischer et al. [25] further improved this approach by incorporating polarized Raman scattering. The aligned fraction as determined by Fischer's method is thus a more accurate indicator of the percentage of aligned CNTs, because Raman scattering strongly discriminates non-CNT impurities in the networks while detecting all nanotubes regardless of crystallinity [26].

In situ X-ray and Raman scattering techniques were employed to monitor the structural evolution of stretch-aligned CNTNs in this study. The experimental results demonstrated in microscale that layered wavy long nanotube ropes/bundles resulted in inhomogeneous alignment in different regions of the network. Thus, an alternative approach of determining the aligned fraction of stretch-aligned networks of long CNT ropes over macroscopic dimensions was studied. The aligned fraction as derived from the measurements of electrical anisotropy of the network and the corresponding X-ray diffraction diagram was proposed for the characterization of alignment in inhomogeneous and macroscopic stretch-aligned CNTNs.

2. Experimental

We used the randomly oriented, commercially available sheets of long MWCNTs manufactured by Nanocomp Technologies Inc. (Concord, NH). The sheets consisted of millimeter-long and small-diameter (3–8 nm) MWCNTs with a range of 2–5 walls, providing an aspect ratio up to 100,000 [27]. Substantial nanotube entanglements and possible interconnections that arose from Nanocomp's proprietary floating catalyst synthesis and aero-gel condense method can be observed in the scanning electron microscope (SEM) image shown in Fig. 1a. The sheets were formed by long spaghetti-like ropes 10–100 nm in diameter. The carbon nanotube sheets were cut into rectangular shapes of 1×4 cm. The samples (2 cm in gauge length) were mounted onto an Anton Paar TS-600 tensile stage, which allowed the *in situ* investigations of the straining process using both X-ray and polarized Raman scattering techniques. The TS-600 stage has a window of 15×15 mm, which allows the X-ray beam to impinge on the sample. However, when used inside the micro-Raman system, the laser beam was not limited to this scope as the stage was mounted with the sample facing the objective lens.

The small angle X-ray scattering (SAXS) and wide angle X-ray diffraction (WAXD) measurements were performed on a Bruker NanoSTAR system with an Incoatec IμS microfocus X-ray source operating at 45 kV and 650 μA. The primary beam was collimated with cross-coupled Göbel mirrors and a pinhole of 0.1 mm in diameter, providing a Cu Kα radiation beam ($\lambda = 0.154$ nm) with a beam size about 0.15 mm in full width half maximum (FWHM) at the sample position. The small-angle scattering intensity was measured on a two-dimensional multiwire Hi-STAR detector. The wide-angle diffraction intensity was captured by a Fuji Photo Film image plate, and read with a Fuji FLA-7000 scanner.

The *in situ* Raman spectroscopic characterization was carried out on a Renishaw inVia micro-Raman system using a 785 nm excitation wavelength (1.58 eV) diode laser. Typical laser power was 0.5 mW with a 50× magnification objective lens, and the laser beam size was around 10 μm. Polarized Raman spectra were obtained in the VV configuration. In order to characterize the inhomogeneity of the CNTNs, an adaptor was custom made to carry the TS-600 tensile stage on a manual Leica two-axis stage in the Renishaw system. The mapping was then obtained from repeated Raman measurements on the sample at 3 mm intervals along the stretch direction and 2 mm intervals in the normal direction.

The anisotropy of electrical resistivity of the CNTNs was measured using the Montgomery method [28]. Similar to the van der Pauw method [29], four copper electrodes were attached at the four corners of the stretched area. The voltage was measured by a Keithley 2182 A Nanovoltmeter between two adjacent electrodes while the current was applied by a Keithley 6221 AC and DC current source between the other two. Similar measurements were then made with all connections rotated by 90° and the current source and voltmeter inverted.

3. Results and discussion

3.1. X-ray scattering

In order to monitor the structural evolution of the CNTNs during mechanical stretching, we carried out simultaneous SAXS and WAXD studies. The SAXS study was performed by scanning the network at different applied strains of 0%, 10%, 20% and 30%, respectively, with a step size of 0.1 mm deformation. The intensities measured by the 2D detector were mapped with pseudo-color, forming the so-called "X-ray nanographs" as shown in Fig. 1d–g. The same color code was used for all four nanographs. It can be seen from each nanograph image that the network was not homogeneous at each stage. However, in general the X-ray scattering intensities increased with higher applied strains, which indicated denser packing of CNTs in the network according to the theories established by Debye et al. [30,31] The observed overall increase in the intensities indicated that instead of eliminating voids during the process, stretching made larger voids break up into smaller ones that are distributed more evenly in between the nanotube ropes. Such a change in the network

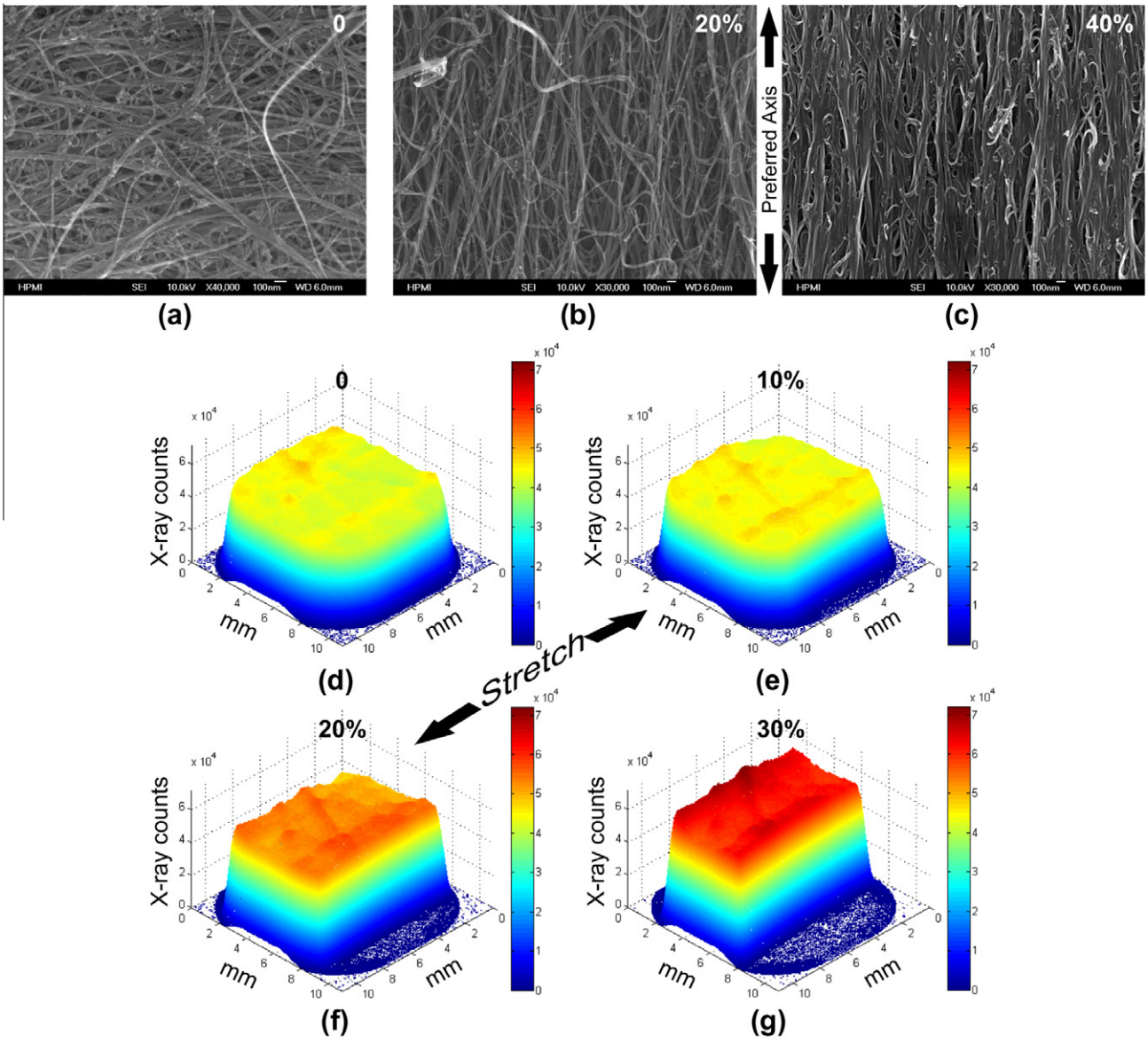

Fig. 1 – SEM images and X-ray nanographs of carbon nanotube networks at different strains: SEM images of networks at strains of 0% (a), 20% (b) and 40% (c); X-ray nanographs at strains of 0% (d), 10% (e), 20% (f) and 30% (g).

morphology is also clearly shown in the SEM images of the CNTN at strains of 20% (Fig. 1b) and 40% (Fig. 1c).

Fischer et al. [25] concluded that the information obtained from X-ray diffraction includes contributions from both the nanotubes and non-nanotube constituents, e.g., voids, metal catalyst, amorphous carbon, etc. The degree of alignment as derived from Hermans orientation function using the X-ray diffraction diagram would thus overestimate the unaligned part of CNTs in the network. However, the mosaic spread of the aligned fraction is accurately given by the X-ray diffraction diagram.

We carried out a simultaneous WAXD study on the CNTNs at the strains of 0%, 20% and 40%. Fig. 2 shows the two-dimensional X-ray diffraction images. The evolution of the anisotropy of the stretch-aligned network can be clearly observed from the arc-shaped (002) peak as the strain increased. However, in order to characterize the long range alignment of nanotube ropes, we summed X-ray counts over the close-packing (CP) peak [32] at the lower angle of $5° < 2\theta < 8°$. As shown in Fig. 3, the FWHM were 42° and 34° at strains of 20% and 40%, respectively. These values of FWHM are later used for determining the aligned fraction of CNTNs using our proposed method.

3.2. *Raman spectra mapping*

Previous studies on polarized Raman measurements show that the G-band peak intensities are strongly dependent on CNT orientation [26,33], thus it has been used extensively for characterizing nanotube alignment [25,34,35]. However, with the laser beam diameter at ~10 μm, this approach only provides accurate information about nanotube orientation

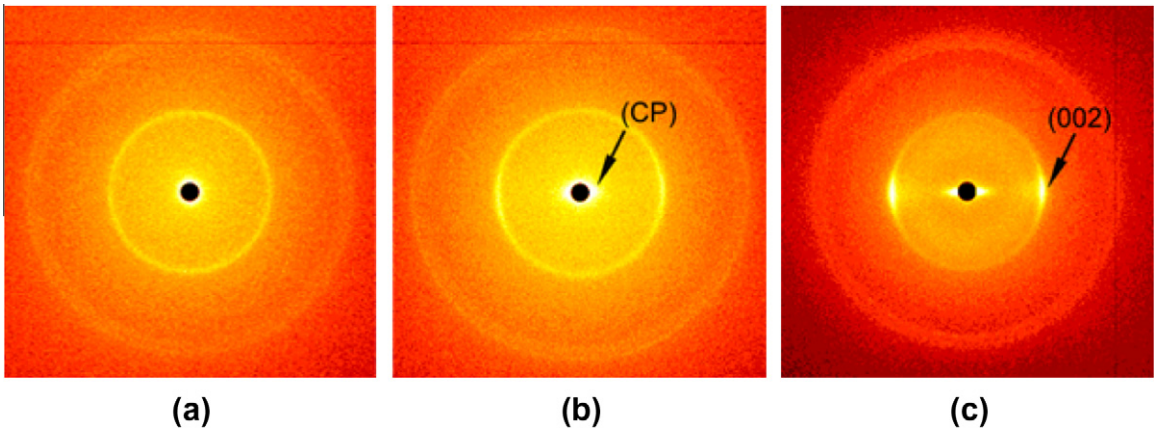

Fig. 2 – Two-dimensional X-ray diffraction images of CNTNs under stretching strains of 0% (a), 20% (b) and 40% (c). The evolution of the anisotropy of (002) and close-packing (CP) peaks is shown.

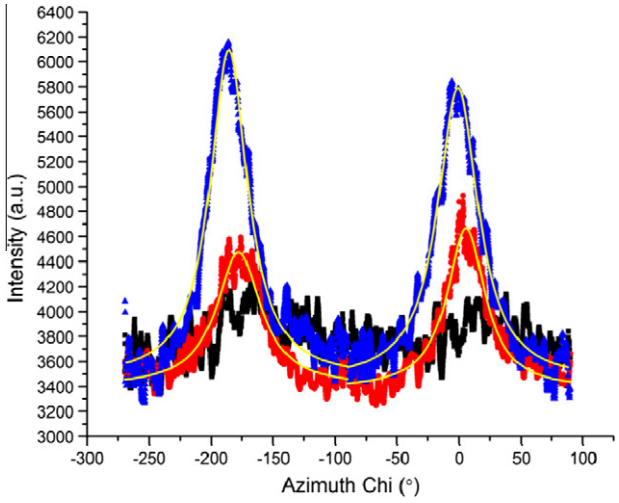

Fig. 3 – X-ray counts summed over intervals $5° < 2\theta < 8°$ about the (CP) peak every 0.1° in X. Black squares, red circles, and blue triangles represent the profiles of the network at strains 0%, 20% and 40%. Yellow curves are the Lorentzian fits (For interpretation of the references to color in this figure legend, the reader is referred to the web version of this article).

within a very limited area that is ~1/200 of the X-ray beam size. Another limitation of Raman spectroscopy is the laser penetration depth. The 532 nm laser was reported to penetrate 150 graphene layers or ~50 nm in depth [36], and the 647 nm laser was also reported to penetrate only the carbon nanotubes near the surface of a CNT rope [26]. For these reasons, researchers either limited the study to bundles smaller than 1 μm [34], or carried out multiple measurements to account for possible inhomogeneity in the degree of alignment of nanotubes at different locations within the aligned network [25,37]. While such inhomogeneity was found to be relatively small (~5%) in nanotubes aligned from filtration in strong magnetic fields [25], mechanical stretching-induced alignment of CNTs was shown to behave otherwise.

We mapped the polarized Raman spectra (VV polarization) of two CNTNs at different strains during stretching. Corresponding intensities of tangential G-band modes that peaked at ~1585 cm^{-1} are shown as the color maps in Fig. 4. Denote Ψ as the angle between the preferred axis and the polarization vector. One network was stretched along the polarization vector ($\Psi = 0$) (Fig. 4a–c), while the other was stretched perpendicular to the vector ($\Psi = 90°$) (Fig. 4d–f). The mapping covered 6×5 points at the interval of 3 mm in the stretch direction and 2 mm in the normal direction, with the exception of Fig. 4c and f where the widths of the networks decreased to ~6 mm at 40% strain.

The randomness of nanotube orientation in the pristine networks can be seen by comparing Fig. 4a and d. The difference between the average intensities of the measurements at $\Psi = 0$ and 90° was within 3%, demonstrating that equivalent amount of nanotube rope segments parallel to the polarization vector was present in both directions. As the strains increased, the trend of intensity change at $\Psi = 0$ started to differ from that at $\Psi = 90°$. When the strain was applied along the polarization vector ($\Psi = 0$), the increase in alignment surprisingly led to decrease in observed intensities near the edges as shown in Fig. 4b and c. We concluded from the phenomenon that the alignment of the wavy long ropes of CNTs was not a straightforward process. Due to the complicacy of entanglements, the value of Ψ for an individual rope was not approaching zero at all times during the process. Meanwhile, the small size and penetration depth of the laser beam determined that only a limited fraction of CNT ropes could be included in the measurements. We speculate that this anomaly was due to the breaking and buckling of nanotube ropes as cracks started to propagate from the edges. This assumption was verified by the trend shown in the mappings at $\Psi = 90°$. As the amount of nanotubes parallel to the polarization vector decreased, the intensities decreased at the strain of 20% (Fig. 4e). However, further increasing the strain to 40%, the intensities on the edge increased (Fig. 4f) in contrast to the decrease in other spots of the network, which may arise from broken ropes that were no longer aligned.

In order to investigate the inhomogeneity of the alignment, the coefficients of variation (CV) of the G-band intensities

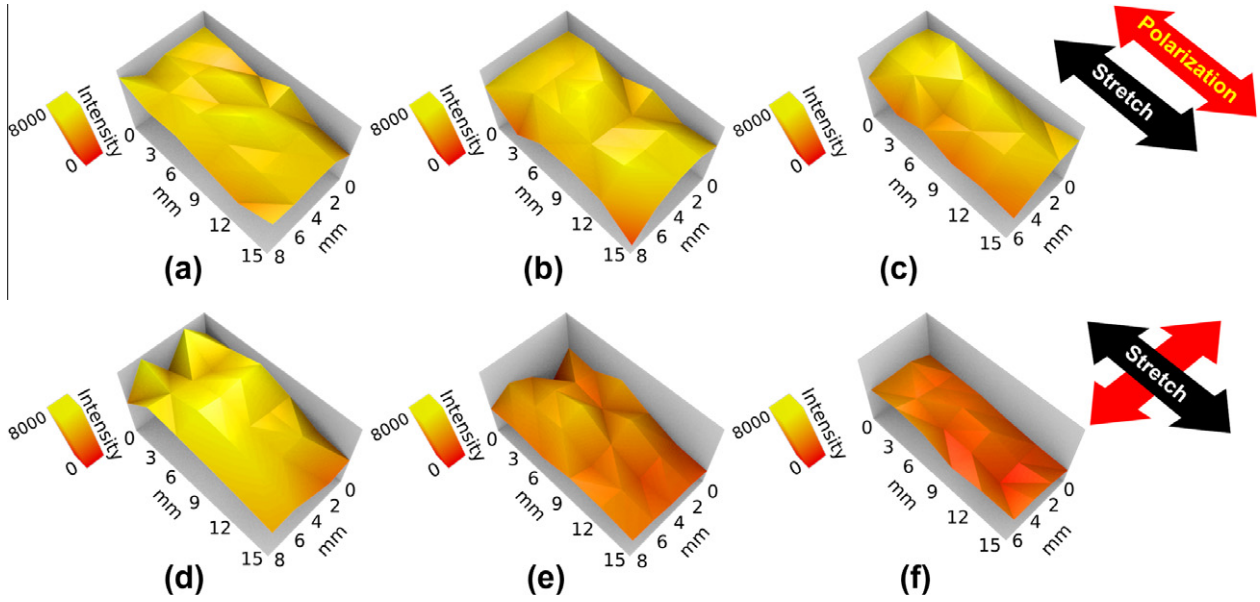

Fig. 4 – Raman mapping of tangential G-band modes of CNTNs under strains of 0%, 20% and 40% along ((a), (b) and (c), respectively) and perpendicular to ((d), (e) and (f), respectively) the direction of the polarization vector. Red arrows indicate the direction of the polarization vector; black arrows show the stretch direction (preferred axis) (For interpretation of the references to color in this figure legend, the reader is referred to the web version of this article).

Table 1 – Coefficient of variation of G-band intensities.

	0%	20%	40%
$\Psi = 0$	12.1	19.9	21.4
$\Psi = 90°$	22.9	27.5	57.5

within each mapping are summarized in Table 1. The large variations of G-band intensities, even in the pristine networks, demonstrated that the laser beam may have only overfilled spots of individual long ropes thus effectively characterizing the local curvatures of the spaghetti-like curves. Such inhomogeneity was greatly suppressed in networks of shorter nanotubes, as the filtration process generated denser structures which allowed more collective sampling within the beam size, where multiple tubes pointed at random directions.

As the strains increased, most of the stretched network would align along the preferred axis, with the exception of the ropes on the edges that started to crack and deviated from the preferred orientation. These two contrary processes gave rise to the increased CV as the strain increased. Compared to the alignment of shorter CNTs in strong magnetic fields where the tubes are rotated to change their orientations toward the preferred axis [38], stretching-induced alignment of long CNT ropes is a fundamentally different process in which the tubes are aligned through straightening the waviness of the spaghetti-like long ropes. Considering the factors of inhomogeneity in alignment, limited laser beam size and penetration depth of Raman scattering, and layered structure of the CNTNs, an approach that is able to characterize the aligned fraction of the long nanotube networks in macroscopic dimensions need to be explored.

3.3. *Anisotropy of electrical resistivity*

Electrical resistivity measurements have the merit of including the bulk of the network under test as a whole. Therefore, the results reflect the collective contribution of all constituent nanotubes over macroscopic dimensions. The anisotropy of the electrical resistivity of aligned CNTNs has been previously studied, and a strong correlation was found between the ratio and the aligned fraction as characterized through polarized Raman scattering [4,25,39]. However, reverse usage of the close relations to determine the aligned fraction is not prevalent because homogeneously aligned networks of shorter CNTs were sufficiently characterized with X-ray and Raman scattering. In order to explore an approach which characterizes inhomogeneous aligned networks in the macroscopic scale, we measured the anisotropy ratio in electrical resistivities to assist X-ray results in calculation of the aligned fraction of CNTNs.

We followed the Montgomery method to carry out the measurements, because the traditional in-line four probe technique can be extraordinarily sensitive to the positioning of the probes if the material demonstrates large anisotropy ratios [28]. The four electrodes were attached to the samples as illustrated in Fig. 5d, where ℓ_1 and ℓ_2 denote the distance between the electrodes along the preferred axis and the perpendicular direction, and ℓ_3 denotes the thickness of the sample. The illustrated setup measures the resistance R_2 along the ℓ_2 direction. The resistance R_1 along the ℓ_1 direction can be measured by rotating all connections by 90°. The Montgomery method then maps the anisotropic sample onto an

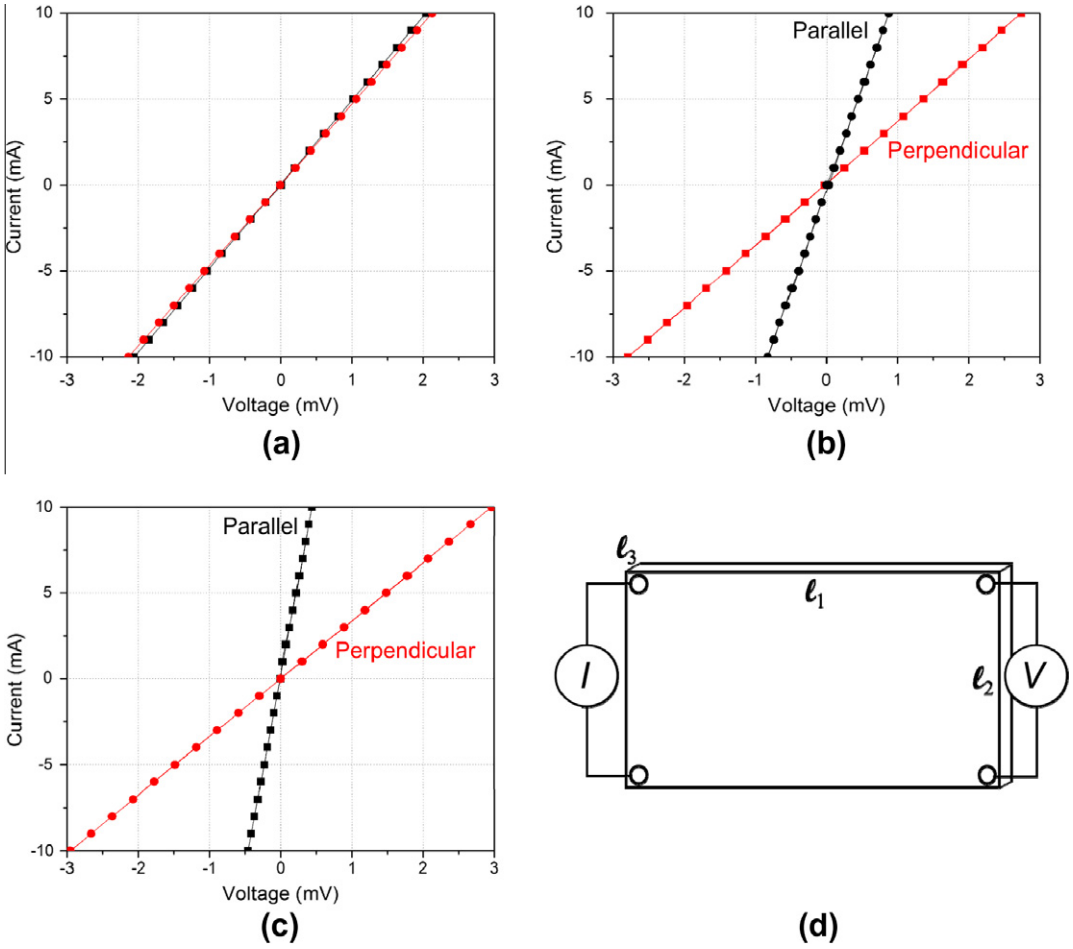

Fig. 5 – Anisotropy of electrical resistivity measured at strains of 0 (a), 20% (b), and 40% (c) using the Montgomery method (d).

Table 2 – Resistivity and anisotropy ratio measured from CNTNs under different strains.

	0%	20%	40%
$\rho_{\perp}$ (Ω cm)	2.5×10^{-3}	7.8×10^{-3}	2.1×10^{-2}
$\rho_{\parallel}$ (Ω cm)	2.4×10^{-3}	2.0×10^{-3}	1.7×10^{-3}
A (anisotropy)	1.04	3.90	12.3

equivalent isotropic sample of dimensions ℓ_1^*, ℓ_2^* and ℓ_3^*, based on the van der Pauw technique [40]. The resistivity values ρ_1 and ρ_2 of the anisotropic material can be solved from

$$\sqrt{\rho_1\rho_2} = H\ell_3 R_2 \quad (1)$$

$$\sqrt{\rho_2/\rho_1} = (\ell_1/\ell_2)\times(\ell_2^*/\ell_1^*) \quad (2)$$

where the ratio ℓ_2^*/ℓ_1^* is obtained from the measured ratio R_2/R_1 using the data of Ref. [26], H is a function of ℓ_1^*/ℓ_2^*, whose values can be found in Ref. [26]. R_2 is the ratio of V/I measured in the setup shown in Fig. 5d.

Table 2 summarizes the measured resistivity values and anisotropy ratios. The trends of resistivity changes in the directions parallel and perpendicular to the preferred axis verifies the assumptions that we made about the structural evolution CNTNs had taken under stretch-induced alignment. As shown in Fig. 6a, the long nanotube ropes in random networks entangle in such a way that they create direct current paths in both directions. After stretch-induced alignment, the straightening and closer packing of the ropes as shown in Fig. 6b dictates that the majority of direct current paths are along the preferred axis. In the perpendicular direction, conduction relies on the tunneling and hopping of carriers between walls within individual MWCNTs as well as between adjacent nanotubes and their ropes. Assuming perfect alignment of nanotubes, the electrical anisotropy of an aligned CNTN should be very similar to that as observed in graphite [41]. The conduction in the preferred axis of aligned CNTNs is similar to that in the basal plane of graphite, and conduction in the perpendicular direction of aligned CNTNs is similar to that through the thickness of graphite. Comparing to the anisotropy ratio that is to the order of 10^3 for graphite [42], the margin for improvement in more effective alignment techniques is still quite large.

3.4. *Determination of the aligned fraction*

The aligned fraction is an indicator of the percentage of nanotubes that are oriented within the FWHM as determined

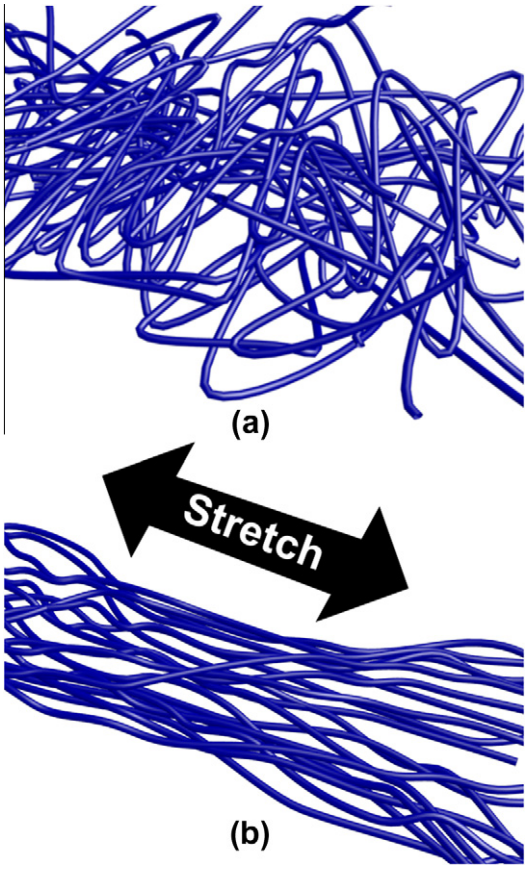

Fig. 6 – Illustration of the structural evolution in networks of long CNT ropes after stretching. Entangled CNT ropes in the pristine network (a) was straightened and more closely packed under tensile strain.

by X-ray scattering. The value is an important input for the structure–property relationship modeling of CNTN structures [43,44]. By modeling an CNTN as an ensemble of 1D conductive rods, Fischer et al. [25] devised the relationship between the anisotropy in electrical resistivities and the orientation distribution function of CNTs as.

$$\frac{\rho_{\perp}}{\rho_{\parallel}} = \left| \frac{\langle \cos(\Psi) \rangle}{\langle |\sin(\Psi)| \rangle} \right|^2 \tag{3}$$

where $\rho_{\perp}$ and $\rho_{\parallel}$ are the resistivities perpendicular and parallel to the stretch direction, respectively. The orientation functions $\langle \cos(\Psi) \rangle$ and $\langle |\sin(\Psi)| \rangle$ are defined as

$$\langle \cos(\Psi) \rangle = \int_{-\pi/2}^{\pi/2} \cos(\Psi) F(\Psi, A, \sigma) d\Psi \tag{4}$$

$$\langle |\sin(\Psi)| \rangle = \int_{-\pi/2}^{\pi/2} |\sin(\Psi)| F(\Psi, A, \sigma) d\Psi \tag{5}$$

where A is the aligned fraction of the CNTN that we attempt to determine, σ is the Gaussian standard deviation, and $F(\Psi,A,\sigma)$ describes the deviation from the perfect alignment of all constituent CNTs:

$$F(\Psi, A, \sigma) = \frac{1 - A}{\pi} + A \frac{1}{\sigma\sqrt{\pi/2}} e^{-2\pi^2/\sigma^2} \tag{6}$$

$$FWHM = \sqrt{2 \ln 2}\sigma \tag{7}$$

Based on the assumption that after stretching, only orientation of the nanotubes changed during the process, the aligned fraction A was solved from Eq. (3) by inserting the values of FWHM that were obtained from the WAXD study, and the anisotropy ratio that was measured by the Montgomery method.

For the pristine network with FWHM = 180° and $\rho_{\perp}/\rho_{\parallel} = 1.0$, the aligned fraction was zero; for the network at the strain of 20% with FWHM = 42° and $\rho_{\perp}/\rho_{\parallel} = 3.9$, the aligned fraction was 0.57; for the network at the strain of 40% with FWHM = 34° and $\rho_{\perp}/\rho_{\parallel} = 12.3$, the aligned fraction was 0.85. In comparison, we also determined the aligned fraction of stretch-aligned CNTNs following the traditional approach through Raman and XRD results. We calculated the corresponding values of aligned fraction to be 0.03, 0.37 and 0.54 for strains of 0%, 20% and 40%, respectively, using the average G-band peak intensities that were measured at each stage. While for the pristine networks, the overestimation by the traditional approach showed the inhomogeneity that existed intrinsically in the CNTNs. The overall underestimation of the aligned fractions in the stretched networks demonstrated the limitations of using Raman spectra in the characterization of layered CNTNs of long carbon nanotube ropes. Deemed as a bulk measurement [25], XRD results were much less limited by the beam size and penetration depth compared to Raman measurements, however the aligned fractions determined by XRD alone were greatly affected by impurities within the CNTNs such as amorphous carbon, metal catalysts, and voids, etc. Such effects of impurities were mitigated in the anisotropy measurements of the electrical resistivities of CNTNs, since the nanotubes were the only material with high aspect ratio within the network: impurities either did not conduct, or equally contributed to the conduction in both directions.

4. Conclusion

This research furthered our early study in an effort to better understand the mechanism of stretch-induced alignment. *In situ* SAXS and WAXD, Raman spectroscopy, and electrical anisotropy measurements were carried out during the stretching process. It was concluded that the process of stretch-induced alignment of CNTNs included straightening the waviness of the long nanotube ropes, self-assembling and denser packing of the nanotubes. Since the alignment fraction over macroscopic dimensions is of great importance to the structure–property relationship studies and the quality control for manufacturing, we proposed an approach that combined the electrical anisotropy and WAXD results to determine the value for stretch-aligned networks of long nanotubes and their ropes.

Acknowledgment

The authors gratefully acknowledge the generous help provided by Mr. Charles Young and Mr. Jerry Horne in making the custom adaptor for the TS-600 stage. This project is supported by AFOSR. The sponsorship and oversight of this program by Dr. Joycelyn Harrison is greatly appreciated.

REFERENCES

[1] Ebbesen TW, Lezec HJ, Hiura H, Bennett JW, Ghaemi HF, Thio T. Electrical conductivity of individual carbon nanotubes. Nature 1996;382(6586):54–6.
[2] Berber S, Kwon YK, Tomanek D. Unusually high thermal conductivity of carbon nanotubes. Phys Rev Lett 2000;84(20):4613–6.
[3] Yu MF, Lourie O, Dyer MJ, Moloni K, Kelly TF, Ruoff RS. Strength and breaking mechanism of multiwalled carbon nanotubes under tensile load. Science 2000;287(5453):637–40.
[4] de Heer WA, Bacsa WS, Chatelain A, Gerfin T, Humphreybaker R, Forro L, et al. Aligned carbon nanotube films - production and optical and electronic properties. Science 1995;268(5212):845–7.
[5] Zhang Y, Iijima S. Elastic response of carbon nanotube bundles to visible light. Phys Rev Lett 1999;82(17):3472–5.
[6] Smith BW, Benes Z, Luzzi DE, Fischer JE, Walters DA, Casavant MJ, et al. Structural anisotropy of magnetically aligned single wall carbon nanotube films. Appl Phys Lett 2000;77(5):663–5.
[7] Chen XQ, Saito T, Yamada H, Matsushige K. Aligning single-wall carbon nanotubes with an alternating-current electric field. Appl Phys Lett 2001;78(23):3714–6.
[8] Kamat PV, Thomas KG, Barazzouk S, Girishkumar G, Vinodgopal K, Meisel D. Self-assembled linear bundles of single wall carbon nanotubes and their alignment and deposition as a film in a dc field. J Am Chem Soc 2004;126(34):10757–62.
[9] Martin CA, Sandler JKW, Windle AH, Schwarz MK, Bauhofer W, Schulte K, et al. Electric field-induced aligned multi-wall carbon nanotube networks in epoxy composites. Polymer 2005;46(3):877–86.
[10] Haggenmueller R, Gommans HH, Rinzler AG, Fischer JE, Winey KI. Aligned single-wall carbon nanotubes in composites by melt processing methods. Chem Phys Lett 2000;330(3–4):219–25.
[11] Jin L, Bower C, Zhou O. Alignment of carbon nanotubes in a polymer matrix by mechanical stretching. Appl Phys Lett 1998;73(9):1197–9.
[12] Frogley MD, Zhao Q, Wagner HD. Polarized resonance Raman spectroscopy of single-wall carbon nanotubes within a polymer under strain. Phys Rev B 2002;65(11):113413.
[13] Bhattacharyya AR, Sreekumar TV, Liu T, Kumar S, Ericson LM, Hauge RH, et al. Crystallization and orientation studies in polypropylene/single wall carbon nanotube composite. Polymer 2003;44(8):2373–7.
[14] Badaire S, Pichot V, Zakri C, Poulin P, Launois P, Vavro J, et al. Correlation of properties with preferred orientation in coagulated and stretch-aligned single-wall carbon nanotubes. J Appl Phys 2004;96(12):7509–13.
[15] Miaudet P, Badaire S, Maugey M, Derre A, Pichot V, Launois P, et al. Hot-drawing of single and multiwall carbon nanotube fibers for high toughness and alignment. Nano Lett 2005;5(11):2212–5.
[16] Li YL, Kinloch IA, Windle AH. Direct spinning of carbon nanotube fibers from chemical vapor deposition synthesis. Science 2004;304(5668):276–8.
[17] Jiang KL, Li QQ, Fan SS. Nanotechnology: spinning continuous carbon nanotube yarns - carbon nanotubes weave their way into a range of imaginative macroscopic applications. Nature 2002;419(6909):801.
[18] Zhang M, Atkinson KR, Baughman RH. Multifunctional carbon nanotube yarns by downsizing an ancient technology. Science 2004;306(5700):1358–61.
[19] Li QW, Zhang XF, DePaula RF, Zheng LX, Zhao YH, Stan L, et al. Sustained growth of ultralong carbon nanotube arrays for fiber spinning. Adv Mater 2006;18(23):3160–3.
[20] Zhang Y, Zou G, Doorn SK, Htoon H, Stan L, Hawley ME, et al. Tailoring the morphology of carbon nanotube arrays: from spinnable forests to undulating foams. ACS Nano 2009;3(8):2157–62.
[21] Cheng Q, Bao J, Park J, Liang Z, Zhang C, Wang B. High mechanical performance composite conductor: multi-walled carbon nanotube sheet/bismaleimide nanocomposites. Adv Func Mater 2009;19(20):3219–25.
[22] Hermans PH. Contribution to the physics of cellulose fibres; a study in sorption, density, refractive power and orientation. Amsterdam; New York: Elsevier Pub. Co., 1946.
[23] Hermans JJ, Hermans PH, Vermaas D, Weidinger A. Quantitative evaluation of orientation in cellulose fibres from the X-ray fibre diagram. Recl Trav Chim Pays-Bas 1946;65(6):427–47.
[24] Liu T, Kumar S. Effect of orientation on the modulus of SWNT films and fibers. Nano Lett 2003;3(5):647–50.
[25] Fischer JE, Zhou W, Vavro J, Llaguno MC, Guthy C, Haggenmueller R, et al. Magnetically aligned single wall carbon nanotube films: preferred orientation and anisotropic transport properties. J Appl Phys 2003;93(4):2157–63.
[26] Gommans HH, Alldredge JW, Tashiro H, Park J, Magnuson J, Rinzler AG. Fibers of aligned single-walled carbon nanotubes: polarized Raman spectroscopy. J Appl Phys 2000;88(5):2509–14.
[27] David S. Lashmore JJB, Jared K. Chaffee, Bruce Resnicoff, Peter Antoinette, inventor systems and methods for formation and harvesting of nanofibrous materials. US patent US 2009/0215344 A1. 2009 2009.
[28] Montgomery HC. Method for measuring electrical resistivity of anisotropic materials. J Appl Phys 1971;42(7):2971–5.
[29] van der Pauw LJ. A method of measuring the resistivity and Hall coefficient on lamellae of arbitrary shape. Philips Tech Rev 1958;20:220–4.
[30] Debye P, Bueche AM. Scattering by an inhomogeneous solid. J Appl Phys 1949;20(6):518–25.
[31] Debye P, Anderson HR, Brumberger H. Scattering by an inhomogeneous solid 2: the correlation function and its application. J Appl Phys 1957;28(6):679–83.
[32] Futaba DN, Hata K, Yamada T, Hiraoka T, Hayamizu Y, Kakudate Y, et al. Shape-engineerable and highly densely packed single-walled carbon nanotubes and their application as super-capacitor electrodes. Nature Mater 2006;5(12):987–94.
[33] Yu ZH, Brus L. Rayleigh and Raman scattering from individual carbon nanotube bundles. J Phys Chem B 2001;105(6):1123–34.
[34] Rao AM, Jorio A, Pimenta MA, Dantas MSS, Saito R, Dresselhaus G, et al. Polarized Raman study of aligned multiwalled carbon nanotubes. Phys Rev Lett 2000;84(8):1820–3.
[35] Rao AM, Jorio A, Pimenta MA, Dantas MSS, Saito R, Dresselhaus G, et al. Comment on "polarized Raman study of aligned multiwalled carbon nanotubes" - reply. Phys Rev Lett 2000;85(16):3545.
[36] Wang YY, Ni ZH, Shen ZX, Wang HM, Wu YH. Interference enhancement of Raman signal of graphene. Appl Phys Lett 2008;92(4):043121.
[37] Casavant MJ, Walters DA, Schmidt JJ, Smalley RE. Neat macroscopic membranes of aligned carbon nanotubes. J Appl Phys 2003;93(4):2153–6.
[38] Walters DA, Casavant MJ, Qin XC, Huffman CB, Boul PJ, Ericson LM, et al. In-plane-aligned membranes of carbon nanotubes. Chem Phys Lett 2001;338(1):14–20.
[39] Inoue Y, Suzuki Y, Minami Y, Muramatsu J, Shimamura Y, Suzuki K, et al. Anisotropic carbon nanotube papers fabricated from multiwalled carbon nanotube webs. Carbon 2011;49(7):2437–43.

[40] van der Pauw LJ. Determination of resistivity tensor and Hall tensor of anisotropic conductors. Philips Res Rep 1961;16:187–95.
[41] Wallace PR. The band theory of graphite. Phys Rev 1947;71(9):622–34.
[42] Tsuzuku T. Anisotropic electrical conduction in relation to the stacking disorder in graphite. Carbon 1979;17(3): 293–9.
[43] Chou T-W, Gao L, Thostenson ET, Zhang Z, Byun J-H. An assessment of the science and technology of carbon nanotube-based fibers and composites. Compos Sci Technol 2010;70(1):1–19.
[44] Jack DA, Yeh CS, Liang Z, Li S, Park JG, Fielding JC. Electrical conductivity modeling and experimental study of densely packed SWCNT networks. Nanotechnology 2010;21(19):195703.